Journal of Materials Chemistry A

PAPER

View Article Online
View Journal | View Issue

Cite this: J. Mater. Chem. A, 2016, 4, 10008

Optimized nitrogen-doped carbon with a hierarchically porous structure as a highly efficient cathode for Na–O_2 batteries†

Jin-ling Ma[ab] and Xin-bo Zhang*[a]

Received 5th April 2016
Accepted 25th May 2016

DOI: 10.1039/c6ta02793h

www.rsc.org/MaterialsA

Development of an efficient air cathode for metal–air batteries composed of an element that is abundant on earth is a scientific and technical challenge. Here, nitrogen (N)-doped carbon cathodes were prepared using two conventional doping methods, namely ammonia activation (ammoxidation) and introduction of an N-containing precursor. Interestingly, the introduction of N-containing precursors to prepare the N-doped carbon material not only gave a different pore distribution with increased surface area but also maintained considerable N content, unlike the use of the ammoxidation method – thus greatly enhancing the catalytic activity (low overpotential) and improving the discharge capacity (6905 mA h g^{-1}) and cycle life (from 8 to 66 cycles) in sodium–oxygen batteries compared with the pure carbon material. This study also stresses the importance of adopting the optimized synthesis method to prepare the N-doped carbon cathode.

Introduction

In recent years, rechargeable light alkali metal–oxygen batteries have caused great attention in the development of large-scale energy storage and electric vehicles because of their high energy density.[1,2] Among them, the sodium–oxygen (Na–O_2) battery has drawn increasing interest since Hartmann reported that a Na–O_2 battery can reversibly discharge/charge at an extremely low overpotential (<200 mV) at room temperature, compared with the most promising lithium–oxygen (Li–O_2) battery (overpotential > 1 V).[3,4] In addition, sodium is an inexhaustible and ubiquitous resource for sustainability development compared to lithium. However, the Na–O_2 battery displays some different problems to the Li–O_2 battery, such as its complicated discharge products,[5,6] and its sensitivity to water (H_2O);[7] however, they also share many common properties, such as the insoluble and isolated products,[8] low energy efficiency,[9] and large charge overpotential when forming thermally stable sodium peroxide (Na_2O_2) which is physically associated with the air cathode.[10] To solve these problems, great research effort has focused on developing an efficient cathode and/or catalysts to improve energy efficiency, lower polarization, and tune and catalyze decomposing discharge products, based on the experience of the Li–O_2 battery;[11] this has included the development of carbon (C)-free cathodes, precious metals, and transition metal oxides catalysts,[12–15] but these cathodes and/or catalysts more or less suffer from low catalytic activity, high cost, or low efficiency. Furthermore, in terms of practical application in metal–oxygen batteries,[16] they are less appealing than carbon-based material. However, pure carbon material always presents a low catalytic activity, so doping a heteroatom into carbon material is used as an effective way to improve its intrinsic catalytic activity.[17–20] Recent studies disclosed that nitrogen (N)-doped graphene showed lower overpotential, higher capacity and longer cycle life compared to the graphene cathode in Na–O_2 batteries.[21] In addition, an N-doped carbon nanotube presented an advantage in the tuning of the morphology of discharge products and improving cycle life compared to the pure carbon nanotube.[22] Theoretical calculations also demonstrated that the strong electron-withdrawing ability of N can cause its neighbouring carbon to be active for the adsorption of O_2 for facilitating the nucleation of discharge products in the oxygen reduction reaction (ORR) process.[23] Furthermore, high surface areas and abundant pore structure are indispensable for the fabrication of the air cathode. It is reported that active sites are always located in a mesoporous (nanoporous) structure, whereas macropores promote simple diffusion of mass towards and away from these active sites, so that the presence of different pore sizes in carbon materials will result in short electron and ion transport paths, as well as enlarging the large active surface areas leading to enhanced catalytic activity.[24,25] In addition, abundant pore structure and surface areas provide adequate space for accommodating discharge products and tackling the deformation resulting from by-product in the metal–air cells.[26,27] Regardless of the great progress that has been made using N-doped carbon

[a]State Key Laboratory of Rare Earth Resource Utilization, Changchun Institute of Applied Chemistry, Chinese Academy of Sciences, Changchun, 130022, P. R. China. E-mail: xbzhang@ciac.ac.cn

[b]University of Chinese Academy of Sciences, Beijing, 100049, P. R. China

† Electronic supplementary information (ESI) available. See DOI: 10.1039/c6ta02793h

material derived from ammonia (NH_3) activating pure carbon material, such as graphene and carbon nanotubes in the Na–O_2 cell, in terms of its practical application, a comprehensive study of the N-doped carbon cathode in optimizing the performance of the Na–O_2 cell is still needed. This is particularly the case with regard to the influence of N content and species, and of the morphology, surface area, and pore-distribution variation of the carbon material, on the capacity, catalytic activity, and cycle life of the Na–O_2 cells.

To reach the goal mentioned above, in this research the N-doped porous carbon cathode was prepared using a simple and economical sol–gel route. In a typical synthesis process, tannic acid and melamine were employed as the carbon and N source, respectively, using different heat treatment temperatures, and thus, N-doped carbon materials were formed *in situ*, with different N contents, species and hierarchical macropore/mesopore structures. As a comparison, tannic acid pyrolyzed under NH_3 (NNC) was used as another method to introduce N. All the previous N-doped carbons, including pure carbon (C) derived from tannic acid, were employed as cathode material and tested in Na–O_2 batteries for the first time. It was demonstrated that a high surface area with optimized N distribution can efficiently improve discharge capacity (6905 mA h g^{-1}) and cycle life (66 cycles), as well as regulate the morphology of the discharge products.

Experimental section

Preparation of material

All the reagents were of analytical grade and were used without further purification. Tannic acid (0.5 g, Beijing Chemical Works) and melamine (2 g, Beijing Chemical Works) were dissolved in 100 mL of distilled water and 100 mL of ethanol, with magnetic agitation for 3.5 h at 95 °C to form a gel, and then the gel was dried at 100 °C overnight. The N-doped carbon was obtained by calcining the gel at 350 °C for 2 h and then pyrolyzing it at 650 °C for 8 h in an argon (Ar) atmosphere and this was designated as NC650 (650 refers to the second pyrolyzing temperature). The NC750 and NC850 were pyrolyzed at 750 and 850 °C, respectively. The pure carbon cathode material, was prepared using the same process without adding melamine and was pyrolyzed at 850 °C. The NNC was obtained using the same process as that used for pure carbon and was pyrolyzed in a flowing NH_3 atmosphere.

Na–O_2 batteries test

The electrochemical tests were carried out in a coin cell 2025 with a 1.0 cm^2 hole placed on the cathode which enabled O_2 to flow in. The cells were assembled in a glove box filled with high-purity Ar (H_2O and O_2 content < 1 ppm). For the cathode preparation, a slurry was obtained by mixing the previous material and poly(vinylidene fluoride) (DuPont Company, 99.9%) in *N*-methyl-2-pyrrolidone (NMP, Aladdin Reagents, AR) with a mass ratio of 9 : 1. The slurry was sprayed on 12 mm carbon paper (CP, TGP-H-060, Toray) with an average loading of 0.5 mg, and then dried in an oven at 90 °C. Sodium and glass fibers were used as the anode and the separator, respectively. The electrolyte was 0.5 M sodium trifluoromethanesulfonate ($NaCF_3SO_3$, Aladdin Reagents, SR) dissolved in tetraethylene glycol dimethyl ether (TEGDME, Aladdin Reagents, AR) with H_2O content < 10 ppm. The cells were discharged to 1.6 V for the first discharge–charge. The cyclic tests were controlled with limited capacity and current density by limiting the discharge cut-off potential to 1.6 V. Cyclic voltammograms (CVs) of the cells were measured between 2.0 and 4.0 V (*versus* Na/Na^+) at a voltage sweep rate of 0.1 mV s^{-1}. Electrochemical impedance spectroscopy (EIS) of the Na–O_2 cell was evaluated using an AC impedance analyzer within a frequency range of 10^6 to 10^{-2} Hz.

Electrochemical tests

All the electrochemical characterization studies were performed in a 0.1 M potassium hydroxide (KOH) solution using a conventional three electrode cell. Silver/silver chloride (Ag/AgCl) and platinum foil were used as reference and counter electrodes, respectively. A rotating disk electrode (RDE) of 5.0 mm in diameter was used as the substrate for the working electrodes. Prior to use, the RDE was polished using aqueous alumina suspensions on felt polishing pads, and then washed with deionized water and ethanol. The catalysts (5 mg) were dispersed in ethanol (1 mL); Nafion solution (50 μL) was then added and mixed ultrasonically for 2 h to obtain a well-dispersed ink. Catalyst ink (0.2 mg cm^{-2} loading) was drop-cast onto the surface of the electrode and then dried at room temperature. Then CV tests were cycled between −1 and 0.2 V at room temperature in N_2- and O_2-saturated 0.1 M KOH, with a scan rate of 50 mV s^{-1}. RDE experiments were carried out in O_2-saturated 0.1 M KOH at room temperature, with a sweep rate of 5 mV s^{-1}, at a speed of 1600 rpm, which was the same as the oxygen evolution reaction (OER), but without the O_2 bubbling.

Characterization

Powder X-ray diffraction (XRD) measurements were performed on a Bruker D8 Focus powder X-ray diffractometer using Cu Kα (λ = 0.15405 nm) radiation (40 kV, 40 mA). Scanning electron microscopy (SEM) was performed on a field emission Hitachi S-4800 instrument, operating at an accelerating voltage of 10 kV and 10 μA with the sample attached on a copper sheet. Transmission electron microscopy (TEM) was performed using a FEI Tecnai G2 S-Twin instrument with a field emission gun operating at 200 kV and the sample was deposited on the copper grid. Fourier transform infrared (FTIR) spectroscopy was performed using a Nicolet 6700 spectrometer. Raman spectra were collected using a Renishaw 2000 confocal microscopy Raman spectrometer with a charge coupled device detector and a holographic notch filter, under ambient conditions. Roughly 5% of the maximum 13 mW laser intensity was applied to prevent carbon damage by the laser. Nitrogen adsorption measurements were performed using a Micromeritics ASAP 2020 adsorption analyser. X-ray photoelectron spectroscopy (XPS) analysis was performed using a VG Scientific (UK) ESCALAB MKII X-ray photoelectron spectrometer. Elemental analysis

(EA) of CHN and O were conducted using a CE Instruments (Italy) EA 1110 element analyser. Conductivity of the carbon material pressed into a wafer was measured using the four-point probe technique, using a RTS-9 (China) four-point meter. The average sheet resistance was based on 20 samples of each material. The CV profile and EIS measurements were performed using a Bio-Logic VMP3 electrochemical workstation. The RDE experiment was performed using a Pine Research Instrumentation MSR electrode rotator. Na–O_2 battery measurements were cycled on a LANDT CT2001A multi-channel battery testing system. Gas chromatography (GC) was performed using a Techcomp GC7900 instrument.

Results and discussion

The pure carbon material and its ammoxidation to N-doped carbon display a lumpy structure, as shown in Fig. 1a. Unexpectedly, N-doped carbon derived from melamine (NC) displays a thin sheet morphology, which is completely different from that of the previous two materials (Fig. S1†). The morphology is loose and possesses some pores, which may result from the release of gases (carbon dioxide, H_2O, and NH_3) during the pyrolyzation of the gel. The TEM image (Fig. 1b) shows a wrinkled sheet structure with some pores, which is beneficial for mass transformation and product deposition. The Brunauer–Emmett–Teller (BET) surface areas of NC obtained with different pyrolysis temperatures, were estimated using N_2 adsorption–desorption isotherms (Fig. 1c), and exhibiting a type-IV isotherm with a steep increase of N_2 absorption at a relatively high pressure, which is indicative of the existence of mesopores. The BET surface areas and pore volumes were found to be 73 $m^2\ g^{-1}$ and 0.47 $cm^3\ g^{-1}$ for NC650 (650 refers to the pyrolysis temperature) sheets, 216 $m^2\ g^{-1}$ and 0.48 $cm^3\ g^{-1}$ for NC750 sheets, and 376 $m^2\ g^{-1}$ and 0.63 $cm^3\ g^{-1}$ for NC850 sheets, respectively. The pore volumes revealed that the NC850 sheets had more mesopores than the NC750 and NC650 ones (Fig. S2†). Obviously, the surface areas and mesopores were increasing with temperature. XPS was performed on NC-based and NNC cathode materials. As shown in Fig. 1d, the N contents were found to be 12.31%, 10.33%, and 6.24% for NC650, NC750, and NC850, respectively, which was consistent with the CHNS element analysis (Table S1†), whereas the NNC had the lowest N content, which indicated that ammoxidation was an inefficient method, compared to using an N-containing precursor, to improve the N content as well as to alter the structure of the carbon material.

Furthermore, the N 1s peaks are deconvoluted into three different types of nitrogen species: pyridinic-N (N1, 398.3 ± 0.1 eV), pyrrolic-N (N2, 399.5 ± 0.1 eV), and graphitic-N (N3, 401.2 ± 0.1 eV). In Fig. 2a, it is apparent that in NC650 N1 and N2 are present; in NC750, N1, N2 and N3 are present, until a temperature of 850 °C is reached; and in NC850 N1 and N3 are present, demonstrating the instability of pyrrolic-N at high temperatures. The three N species also exist in NNC. Additionally, the Raman spectra reveal that pure carbon material has the lowest intensity ratio (I_D/I_G), implying that there was a relatively low structural defect because of the decreased oxygen at the high pyrolytic temperature, whereas the I_D/I_G increased after introducing the N precursor, but gradually decreased as the temperature increased (Fig. 2b), which is consistent with the N content, demonstrating that the higher the N content, the more defects there were, which was beneficial for catalysis.

To evaluate the performance of the N-doped carbon materials in the Na–O_2 battery, they were sprayed on CP including pure carbon material and then examined in 0.5 M $NaCF_3SO_3$ in TEGDME electrolyte. Fig. 3a displays the first discharge–charge curves with the five cathodes at a current density of 200 mA g^{-1}. NC750 showed the highest discharge potential of these five cathodes. Its charge curve also demonstrates three charge plateaus, at 2.37, 3.20 and 3.90 V, which according to previous reports[28] correspond to the oxidation of sodium superoxide (NaO_2), Na_2O_2 and by-products, but the other cathodes almost demonstrate two charge potential plateaus with a short region of NaO_2 decomposition. This phenomenon is also confirmed by the CV profiles, where the N-doped carbon cathodes derived from melamine demonstrate a lower oxygen evolution potential

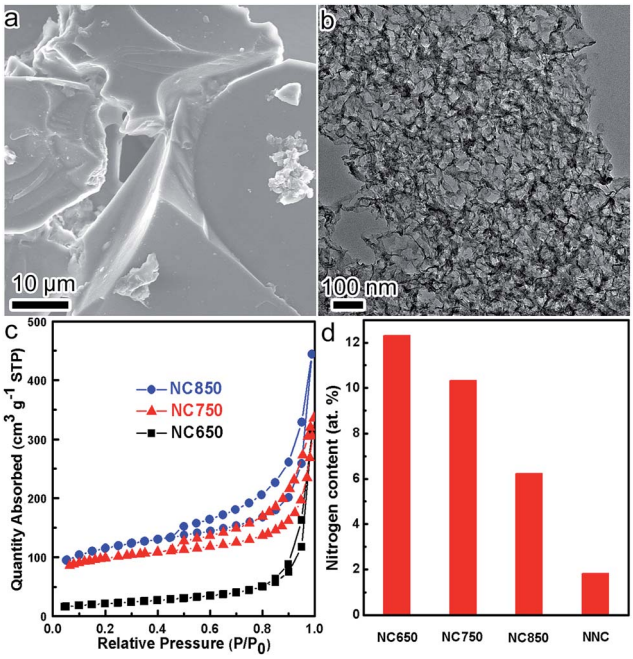

Fig. 1 (a) SEM image of the C and NNC, and TEM image (b), N_2 adsorption–desorption isotherms (c), and nitrogen content (d) of the NC-based materials.

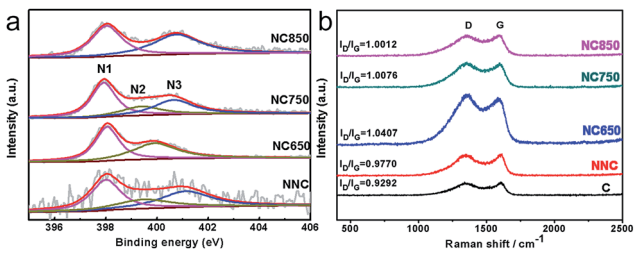

Fig. 2 High resolution N 1s spectra (a), and Raman spectra (b) for NNC, NC650, NC750, NC850 and C.

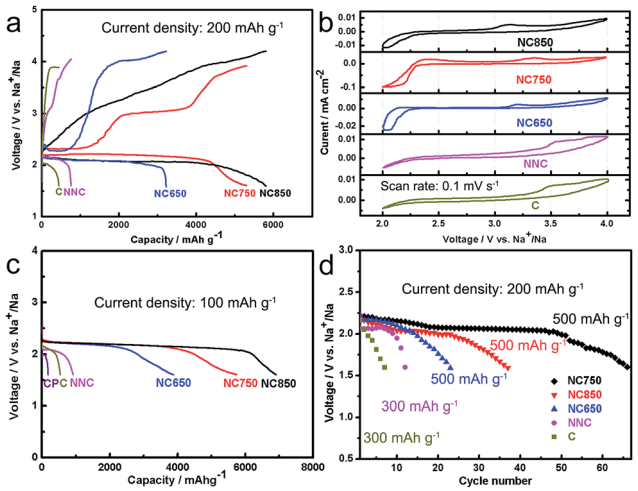

Fig. 3 First discharge–charge curves at a current density of 200 mA g^{-1} (a), CV profiles at a voltage sweep rate of 0.1 mV s^{-1} (b), discharge capacity at the current density of 100 mA g^{-1} (c), and voltage of the terminal discharge *versus* the cycle number (d) for Na–O_2 batteries with C, NNC, NC650, NC750, and NC850.

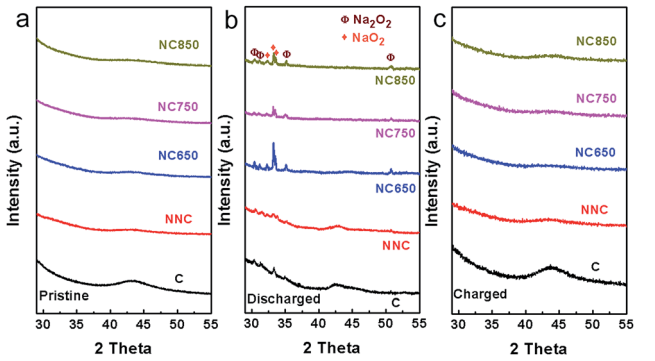

Fig. 4 XRD patterns of the pristine (a), discharged (b), and charged (c) cathodes of C, NNC, NC650, NC750, and NC850 in Na–O_2 batteries.

than pure carbon and ammoxidized carbon ones (Fig. 3b). In addition, the NC750 cathode clearly reveals the oxidation of NaO_2 at 2.34 V in the CV profile, which confirmed its superiority among these cathodes in forming and decomposing NaO_2. Furthermore, despite the low N content in NNC, it still displayed a slightly higher OER potential than pure carbon, which fully indicates the advantage of nitrogen introduction for catalysing the sluggish ORR and OER in Na–O_2 batteries. The discharge capacity of these cathodes, including CP at a current density of 100 mA g^{-1}, is shown in Fig. 3c. CP was used here to exclude the capacity contribution of the current collector. It is well known that the discharge capacity of the Na–O_2 batteries is tightly related to the surface areas of the cathode. NC850 undoubtedly delivers the highest capacity because of its dominant surface areas for accommodating discharge products, but this advantage is slightly better than the NC750 one when considering that the surface area of NC750 is far less than that of NC850. Cyclability is another important criterion to evaluate the performance of Na–O_2 batteries. In this case, for avoiding the overgrowth of discharged products induced by deep discharge, the cycle life was tested using a confined capacity of 500 mA h g^{-1} and 300 mA h g^{-1} for the NC-based and the other two cathodes, respectively, at a current density of 200 mA g^{-1} (Fig. 3d). The trend of the cycle life is NC750 > NC850 > NC650 > NNC > C, and with the NC750 cathode, the Na–O_2 cell achieves 66 cycles, and this represents the best of the carbon-based cathodes reported up until now when the mixture of NaO_2 and Na_2O_2 dominate the discharge products (Table S2†).

The cycle life is closely associated with the electrochemical reversibility of discharge products and side products, so the reversibility of discharge products was tracked during the first discharge–charge process. XRD patterns were used to verify that the discharge products were a mixture of Na_2O_2 and NaO_2 (Fig. 4b and S3†), which is consistent with the results from a previous study.[27] After charging, all the cathodes returned to the initial state. No other phases of products were detectable (Fig. 4a and c), thus showing observable reversibility, but this was not enough to confirm that there were no side products and complete reversibility of the discharge products.

Then, the SEM images of the discharge products on these cathodes during cycling were recorded. After discharge, large microscale spherical particles were prone to form on pure carbon and NNC cathodes (Fig. 5a and b), whereas smaller nanoscale particle products were uniformly deposited on the NC-based cathode (Fig. 5c–e). This may be because of the presence of sufficient active sites on the high surface areas of the graphene-like NC-based cathode to promote the formation of nanosized discharge products. It was reported that nanosized discharge products were easy to decompose.[29] After charging, less products were observed on the charged NC-based cathodes, especially on the NC750 one, than on the pure carbon and NNC ones, demonstrating their high catalytic activity toward decomposition of discharge products, as shown in Scheme S1.†

FTIR spectroscopy was used as a sensitive detection method and was also employed to characterize the discharge products. Compared with the pristine cathode in Fig. S4a,† after discharging there was an additional peak located at 1442 cm^{-1},

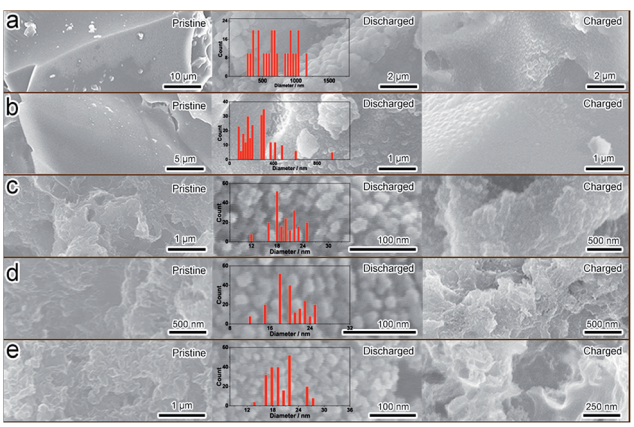

Fig. 5 SEM images of the C (a), NNC (b), NC650 (c), NC750 (d), and NC850 (e) cathodes in Na–O_2 batteries at different discharge–charge states (insert: histogram of the discharge product size distribution).

which was attributed to the characteristic Na_2O_2 peak (Fig. S4b†). After charging, this peak disappeared on the NC-based cathode, whereas the red shift to 1456 cm^{-1} on the C and NNC cathodes (Fig. S4c†) demonstrated the existence of undecomposed sodium carbonate. This phenomenon was also found in Li–O_2 batteries, where the carbonate was from electrolyte decomposition.[30] The reason for the previous XRD detecting no undecomposed discharge products on the C and NNC cathodes after charging may be because of the formation of noncrystalline or low-intensity undecomposed products.

Subsequently, EIS was used to determine the change of the resistance of the Na–O_2 batteries during the discharge–charge process. Before discharge, the cell with a pure carbon cathode had the lowest charge-transfer resistance (R_{ct}) corresponding to the depressed semicircle in EIS at high frequencies (Fig. S5a†), and this was because of its highest conductivity with a low oxygen content at 850 °C. The NC650 one has the highest resistance because of the high content of electronegative heteroatoms, such as oxygen and nitrogen, at a low heat treatment temperature, which is consistent with the electronic conductivity displayed in Table S3.† After discharging to the same capacity, the insoluble and isolated discharge products deposited on these cathodes cause the R_{ct} to increase, just as previously reported (Fig. S5b†).[31] Among the cathodes, NC750 increases a little, for which the rational explanation is the formation of partial poor crystalline discharge products, just as Yilmaz *et al.* previously reported.[32–34] It was reported that decomposition of poor crystalline discharge products needs less energy than that of crystalline products, thus explaining the low charge potential with the NC750 cathode in Na–O_2 batteries. After charging, the R_{ct} of all these cathodes decreased compared with the discharged ones, which demonstrated the decomposition of the discharge product (Fig. S5c†). Apparently, the Rct of NC-based cathodes, especially that of NC750, almost return to the initial state, demonstrating the best recovery among the three cathodes, and less undecomposed product on it, whereas the Rct of the pure carbon and NNC ones compared with the initial apparent increase, which was consistent with the observations from the SEM images and the FTIR results. This reveals that the relatively numerous active sites and the N content of the extensive surface area of the highly conductive NC750 cathode efficiently catalyse the decomposition of discharge products, thus greatly inhibiting the accumulation of products on the cathode and improving the cycle life of the Na–O_2 cell. The GC result (Fig. S6†) shows that the cell with the NC750 cathode has less side reactions.

The ORR catalytic activities of the as-prepared samples were also investigated in 0.1 M KOH solution. As shown in Fig. S7,† no obvious redox peak was observed for the five samples in N_2-saturated solution. In contrast, when the solution was saturated with O_2, a well-defined cathodic peak clearly appeared in these samples, confirming the electrocatalytic activity for ORR (Fig. S7a–e†). Compared with the other samples, the more positive ORR peak potential of NC750 suggested its superior activity. The highest onset potential and largest cathodic current density were also obtained using NC750 (Fig. S7f and Table S4†), which demonstrated that the optimized nitrogen content, species, and porous structure of the N-doped carbon materials play a critical role in catalysis. Subsequently, the OER catalytic activity was also determined (Fig. S8 and Table S4†). This demonstrated that NC750 achieves the most negative onset potential and lowest Tafel slope among these materials, thus showing its superiority for OER.

Conclusions

In conclusion, two methods were adopted for doping N into carbon material. The results show that N-doped carbon derived from an N-containing precursor not only increases the N content, but also improves the surface areas by formation of different-sized pores. Whereas ammoxidation hardly alters the morphology of carbon and only achieves a lower N content compared with adopting a N-containing precursor under identical synthesis conditions, giving a limited improvement of catalytic activity. Further examination of the Na–O_2 battery revealed the optimized N content and pore distribution at temperatures beneficial for ORR and OER (low overpotential), as well as improving cycle life (from 8 to 66 cycles), compared with a pure carbon cathode. In addition, it can control the morphology of discharge products on discharge and then efficiently catalyse their decomposition whilst charging. Clearly, the research on the application of N-doped carbon as cathode materials for Na-O_2 battery should be deepened, by optimizing its preparation through selection of an appropriate N-containing precursor, heat treatment temperature and methodology.

Acknowledgements

This work was financially supported by the 100 Talents Program of the Chinese Academy of Sciences, the National Program on Key Basic Research Project of China (973 Program, Grant no. 2012CB215500 and 2014CB932300), and the National Natural Science Foundation of China (Grant no. 21101147, 21203176, and 51301160).

References

1 K. M. Abraham and Z. Jiang, *J. Electrochem. Soc.*, 1996, **143**, 1.
2 E. Peled, D. Golodnitsky, H. Mazor, M. Goor and S. Avshalomov, *J. Power Sources*, 2011, **196**, 6835.
3 P. Hartmann, C. L. Bender, M. Vračar, A. K. Dürr, A. Garsuch, J. Janek and P. Adelhelm, *Nat. Mater.*, 2013, **12**, 228.
4 P. Adelhelm, P. Hartmann, C. L. Bender, M. Busche, C. Eufinger and J. Janek, *Beilstein J. Nanotechnol.*, 2015, **6**, 1016.
5 Y. Hu, X. Han, Q. Zhao, J. Du, F. Cheng and J. Chen, *J. Mater. Chem. A*, 2015, **3**, 3320.
6 C. L. Bender, D. Schröder, R. Pinedo, P. Adelhelm and J. Janek, *Angew. Chem., Int. Ed.*, 2016, **55**, 4640.
7 Q. Sun, H. Yadegari, M. N. Banis, J. Liu, B. Xiao, X. Li, C. Langford, R. Li and X. Sun, *J. Phys. Chem. C*, 2015, **119**, 13433.
8 Z. Jian, Y. Chen, F. Li, T. Zhang, C. Liu and H. Zhou, *J. Power Sources*, 2014, **251**, 466.

9 B. D. McCloskey, R. Scheffler, A. Speidel, D. S. Bethune, R. M. Shelby and A. C. Luntz, *J. Am. Chem. Soc.*, 2011, **133**, 18038.
10 J. Kim, H. D. Lim, H. Gwon and K. Kang, *Phys. Chem. Chem. Phys.*, 2013, **15**, 3623.
11 A. Kushima, T. Koido, Y. Fujiwara, N. Kuriyama, N. Kusumi and J. Li, *Nano Lett.*, 2015, **15**, 8260.
12 W. Liu, Q. Sun, Y. Yang, J. Y. Xie and Z. W. Fu, *Chem. Commun.*, 2013, **49**, 1951.
13 S. Zhang, Z. Wen, K. Rui, C. Shen, Y. Lu and J. Yang, *J. Mater. Chem. A*, 2015, **3**, 2568.
14 S. Rosenberg and A. Hintennach, *J. Power Sources*, 2015, **274**, 1043.
15 W. M. Liu, W. W. Yin, F. Ding, L. Sang and Z. W. Fu, *Electrochem. Commun.*, 2014, **45**, 87.
16 I. Landa-Medrano, C. Li, N. Ortiz-Vitoriano, I. Ruiz de Larramendi, J. Carrasco and T. Rojo, *J. Phys. Chem. Lett.*, 2016, **7**, 1161.
17 J. Ryu, N. Jung, D. H. Lim, D. Y. Shin, S. H. Park, H. C. Ham, J. H. Jang, H. J. Kim and S. J. Yoo, *Chem. Commun.*, 2014, **50**, 15940.
18 W. J. Lee, U. N. Maiti, J. M. Lee, J. Lim, T. H. Han and S. O. Kim, *Chem. Commun.*, 2014, **50**, 6818.
19 Y. Zheng, Y. Jiao, L. Ge, M. Jaroniec and S. Z. Qiao, *Angew. Chem., Int. Ed.*, 2013, **52**, 3110.
20 L. F. Chen, Z. H. Huang, H. W. Liang, W. T. Yao, Z. Y. Yu and S. H. Yu, *Energy Environ. Sci.*, 2013, **6**, 3331.
21 Y. Li, H. Yadegari, X. Li, M. N. Banis, R. Li and X. Sun, *Chem. Commun.*, 2013, **49**, 11731.
22 Q. Sun, H. Yadegari, M. N. Banis, J. Liu, B. Xiao, B. Wang, S. Lawes, X. Li, R. Li and X. Sun, *Nano Energy*, 2015, **12**, 698.
23 Y. Jing and Z. Zhou, *ACS Catal.*, 2015, **5**, 4309.
24 P. Trogadas, V. Ramani, P. Strasser, T. F. Fuller and M. O. Coppens, *Angew. Chem., Int. Ed.*, 2016, **55**, 122.
25 B. Zhao and M. M. Collinson, *Chem. Mater.*, 2010, **22**, 4312.
26 C. Shu, Y. Lin and D. Su, *J. Mater. Chem. A*, 2016, **4**, 2128.
27 H. Yadegari, M. N. Banis, B. Xiao, Q. Sun, X. Li, A. Lushington, B. Wang, R. Li, T. K. Sham, X. Cui and X. Sun, *Chem. Mater.*, 2015, **27**, 3040.
28 H. Yadegari, Y. Li, M. N. Banis, X. Li, B. Wang, Q. Sun, R. Li, T. K. Sham, X. Cui and X. Sun, *Energy Environ. Sci.*, 2014, **7**, 3747.
29 W. J. Kwak, Z. Chen, C. S. Yoon, J. K. Lee, K. Amine and Y. K. Sun, *Nano Energy*, 2015, **12**, 123.
30 J. J. Xu, Z. L. Wang, D. Xu, L. L. Zhang and X. B. Zhang, *Nat. Commun.*, 2013, **4**, 2438.
31 K. Hayashi, K. Shima and F. Sugiyama, *J. Electrochem. Soc.*, 2013, **160**, A1467.
32 E. Yilmaz, C. Yogi, K. Yamanaka, T. Ohta and H. R. Byon, *Nano Lett.*, 2013, **13**, 4679.
33 Y. Yang, W. Liu, Y. Wang, X. Wang, L. Xiao, J. Lu and L. Zhuang, *Phys. Chem. Chem. Phys.*, 2014, **16**, 20618.
34 F. Tian, M. D. Radin and D. J. Siegel, *Chem. Mater.*, 2014, **26**, 2952.